Ethane-xenon mixtures under shock conditions

Rudolph J. Magyar, Seth Root, Kyle Cochrane, Thomas R. Mattsson, and Dawn G. Flicker

Phys. Rev. B **91**, 134109 — Published 22 April 2015

DOI: 10.1103/PhysRevB.91.134109

Ethane-xenon mixtures under shock conditions

Rudolph J. Magyar, Seth Root, Kyle Cochrane, Thomas R. Mattsson, and Dawn G. Flicker
Sandia National Laboratories, Albuquerque, New Mexico, 87185, USA.
(Dated: February 11, 2015)

Mixtures of light elements with heavy elements are important in inertial confinement fusion. We explore the physics of molecular scale mixing through a validation study of equation of state (EOS) properties. Density functional theory molecular dynamics (DFT-MD) at elevated-temperature and pressure is used to obtain the thermodynamic state properties of pure xenon, ethane, and various compressed mixture compositions along their principal Hugoniots. To validate these simulations, we have performed shock compression experiments using the Sandia Z-Machine. A bond tracking analysis correlates the sharp rise in the Hugoniot curve with the completion of dissociation in ethane. The DFT-based simulation results compare well with the experimental data along the principal Hugoniots and are used to provide insight into the dissociation and temperature along the Hugoniots as a function of mixture composition. Interestingly, we find that the compression ratio for complete dissociation is similar for several compositions suggesting a limiting compression for C-C bonded systems.

PACS numbers: 62.50.Ef, 71.15.Pd, 71.30.+h

I. INTRODUCTION

Understanding the behavior of mixtures under intense dynamic loading conditions is needed for designing inertial confinement fusion (ICF) targets. Hydrodynamic mixture of the imploding capsule into deuterium fuel plays a significant role in the formation of hot spots affecting the neutron yield.[1–3] For example, hotspot formation is important in the High-Foot Program[4–6] that seeks to achieve higher yields with carefully designed pulses. The complicated computer simulations of these dynamic events rely on accurate equation of state models (EOS) for pure and mixed materials that span a broad range of temperatures, pressures, and densities. Critical to the quality of EOS models is the fidelity of underlying data, both experimental and calculated.

During impact/implosion situations, pure materials will often dynamically mix, and a new model for the mixed material is required. The most extreme limit of mixing is full homogenization on the molecular scale. This is the final stage of a hydrodynamic mix and where one would expect the most significant interspecies interactions, resulting in the largest deviations from models based on isolated species. We present a joint experimental and simulation study of an atomic scale mixture under the relevant pressures and temperatures for these targets.

We examine thermally equilibrated and homogenized molecular mixing. As a controlled case, we study the miscible cryogenic liquid mixtures of xenon and ethane (C_2H_6). This combination is amenable to experiments because mixtures can be attained with modest pressures and liquid nitrogen cooling and the initial states of the pure and mixed liquids are well-characterized. The mixture is also a good proxy for the polymer liners and heavier elements that might be used in fuel capsules on the National Ignition Facility and other Inertial Confinement Fusion targets.[7,8] Previous studies of the isolated species have found good agreement between experiment and theory.[9–11] Since we expect significant interspecies interactions for molecular-scale mixtures, it is not immediately obvious that computations of the mixtures will be as accurate as pure species simulations. We calculate the Hugoniots of various Xe-ethane mixtures using DFT-MD and compare the results to Hugoniot data from flyer plate experiments using Sandia's Z-Machine.

Once validated, simulations provide additional insight into the physical properties of materials. For shock compression experiments, temperature is difficult to measure. This quantity comes naturally in the DFT-MD simulations, and a validation study of the pressures and compression ratios adds support that the predicted temperatures are reliable. An important feature in the Hugoniot data of reactive systems is the onset and completion of molecular dissociation. Often at the onset of dissociation, a change in slope or a plateau is observed in the Hugoniot data. After molecular dissociation, the number of uncorrelated ions increases causing the pressure to rise and the Hugoniot to show significant steepening. Upon complete dissociation small changes in the shock compressed density result in precipitous increases in the pressure.[12–15] However, a possible competing effect is exotic bonding such as the formation of Xe-bonds under pressure.[16] Through a bond tracking analysis we can determine the stoichiometric ratios of various products to characterize the interspecies chemistry along the Hugoniot. This allows us to compare changes in the shape of the Hugoniot curve to chemical changes within the sample.

This paper is organized into 3 sections. In the first, we discuss some of the details and convergence criteria used in the DFT-MD simulations. The second section describes the experimental setup on the Z-Machine, and the third section provides analysis of the combined simulation and experimental results.

II. DENSITY FUNCTIONAL / QUANTUM MOLECULAR DYNAMICS SIMULATIONS

In DFT-MD, the nuclei are moved on the Born-Oppenheimer potential-energy surface of thermally excited electrons. The DFT method is outlined in Refs. 17–19. The DFT-MD simulations were performed with VASP 5.2,[20–22] a plane-wave, periodic-boundary-conditions code that employs projector augmented-wave (PAW) core functions.[23,24] We use stringent convergence criteria as described in Ref. 25. Specifically, a 900 eV plane-wave cut off was chosen to converge the pressure within 1%. 8 electrons for Xe, 4 for C, and 1 for H are treated explicitly. The time steps are between 1.0 and 0.1 fs depending on the temperature. Typical run times were on the order of 4 ps after initial thermalization. The simulations are performed in the NVT ensemble (fixed number of atoms and fixed volume/density at prescribed temperature). We employ velocity scaling as the thermostat for the simulations; however, additional simulations using an Nose-Hoover thermostat show negligible difference for Hugoniot states. Complex k-point sampling with the Baldereschi mean-value point is applied because its accuracy and efficiency for disordered structures at high temperature[26]. We run Mermin's finite temperature formulation of DFT with ground-state exchange correlation functionals,[19] shown to be critical for high energy-density applications.[27] We report the results for only AM05,[28,29] which is particularly well-suited to describe compressed solids and liquids.[11] Results within the local density approximation (LDA) are comparable.

A direct route to compare experimental shock data to DFT-MD simulations is through the calculation of Hugoniot states. The hydrostatic Hugoniot condition can be expressed as $2(E-E_{ref}) = (P+P_{ref})(V_{ref}-V)$ where E is the internal energy per mass, P is the system pressure, and V is the specific volume and is related to the inverse of the mass density, $V = 1/\rho$. The subscript *ref* refers to the reference state, which is at the initial conditions of the experiment.

Each simulation was allowed to equilibrate at a constant temperature and density for multiple picoseconds or until the block averaged[30] standard deviation of the mean was less than 1%. At each density, we used two temperatures to approximate the Hugoniot relation; one temperature such that the pressure and energy were too high and the other too low. We then interpolated between them to obtain the Hugoniot pressure, energy, and temperature. For higher compression points along the Hugoniot, an alternative approach is possible in which several densities at fixed temperatures are performed and used to locate the Hugoniot state.

Throughout, we reserve x for the mass mixing ratio defined as

$$x = \frac{n_{ethane} M_{ethane}}{n_{Xe} M_{Xe} + n_{ethane} M_{ethane}} \quad (1)$$

where n is the number density of molecules (atoms) and M is the molecular mass of each species. This form is convenient because EOS tables are often given in terms of mass densities.

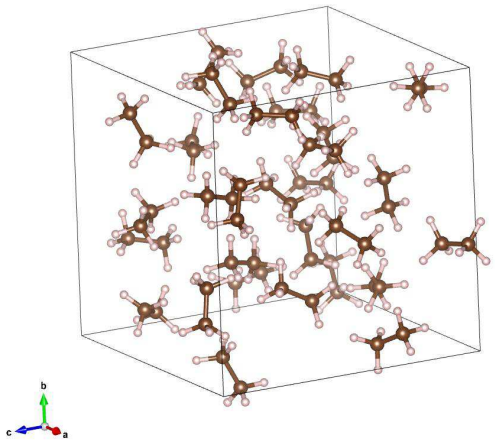

FIG. 1. Snapshot of the liquid ethane reference state nuclear positions within a super-cell at density $\rho = 0.571\ g/cm^3$at 163 K from a DFT-MD AM05 calculation. C atoms are brown and H atoms are white.

The reference state (E_{ref}, P_{ref}, and V_{ref}) for ethane, Fig. 1, was chosen to closely match experimental initial conditions of 0.571 $g/cm^3$and 163 Kelvin determined from cryomixture data.[31] For the 50/50 molar mixing $x = 0.19$, the reference state at 163K and P $<$ 10 kBar is $\rho_{ref} = 1.676\ g/cm^3$and is shown in Fig. 2. For the 50/50 mass mixing $x = 0.5$, the reference state at 163K and P $<$ 20 kBar is $\rho_{ref} = 0.960\ g/cm^3$. The densities are taken to be given for the reference state and we do not perform calculations to optimize over density at ambient pressure. The results for pure xenon are reported in a previous validation study.[11]

A computer code was created to position atoms within a super cell to represent the Xe-Ethane mixture. The center of mass positions of the ethane molecules were chosen to uniformly fill a super cell with 2^3, 3^3, and 4^3 ethane molecules. To achieve a desired mix ratio x, a number of ethane molecules were randomly substituted with Xe. It was found that the largest super cell (4^3)was impractical for more than a few simulations. The $3\times3\times3$ supercell was converged with respect to simulation size at 1 MBar. Note that changing the density was done adiabatically by gradually adjusting the super cell size, running a dynamic DFT-MD simulation to allow transient vibrational modes to dissipate, and then adjusting further. A sudden large density scaling would strain bonds, increasing the system energy too dramatically and result in premature bond breaking. We determined that 27 ethane molecules in each super-cell is sufficient by performing simulations with larger super-cells. We found

that simulating 64 molecules at 0.8, 1.1, 1.2, 1.5, and 1.8 g/cm^3provided nearly identical results for pressure and energy compared to 27 molecule analogs. The large super-cell simulations gave the same Hugoniot points to within $\leq$ 0.5% in pressure. The number and type of atoms in each super-cell varies according to the mix ratio. The 50/50 mass mix ($x = 0.5$) had 5 Xe and 22 ethane molecules (5 Xe, 44 C 132 H) for a total of 181 atoms. The 50/50 molar mix ($x = 0.19$, see Fig. 2 had 13 Xe and 13 ethane (13 Xe, 26 C and 78 H) for a total of 117 atoms.

We address the degree of dissociation using a bond tracking analysis on the nuclear positions.[15] Two elements are considered bonded if they are within a defined bonding radius for at least as long as a defined persistence time. For the results quoted here, we choose a persistence time of 100 fs (for scale, this corresponds to approximately 5 inverse vibrational frequency time scales for the C-C bond). More importantly, the time is long enough that if two atoms are not bonded, they have ample opportunity to drift apart. Time step can also affect dissociation. If a time step is too large, an atom can move farther than would be realistic and prematurely dissociate. We have found that 0.1 to 1.0 fs (decreasing as temperature increases) tends to work well for hydrocarbons. The bond lengths we use are obtained from the maximum value of the nearest-neighbor distribution of the pair correlation function for C-C and C-H[15] calculated just prior to dissociation on the Hugoniot. The values are slightly longer than the equilibrium bond lengths because we use an explicit time step and must take into account the discrete atomic vibration. It should be noted that equilibrium bond lengths are the average and not the extremes; bond lengths may increase slightly with temperature. By defining a slightly larger than equilibrium bond length, we can use a consistent set of parameters when analyzing a variety of simulations. We use Xe-Xe 0.25 Å, Xe-C 2.0 Å, Xe-H 2.0 Å, C-C 1.68 Å, C-H 1.28 Å, and H-H 0.8 Å. Since Xe-Xe bonding is unlikely, we chose an arbitrarily small bond cut-off. Alternate approaches to bond tracking exist in the literature that reduce the number of free parameters[32,33]; however, these have been applied to two species situations and eliminate the need to set bond radii by tracking nearest neighbors. In the case of Xe-ethane mixtures, we have the possibility of single and double bonds and nearest neighbor analysis could conceivably under-represent the number of bonds.

Results from the DFT simulations are listed in Tables I-III and are compared to the experimental data in Section IV.

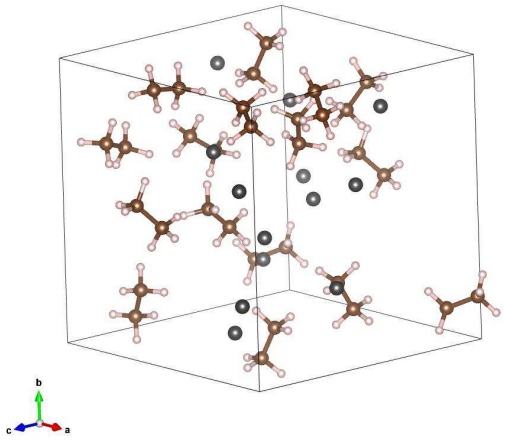

FIG. 2. Same as Fig. 1, but now including Xe with mass ratio x=0.19 and density $\rho = 1.676$ g/cm^3. Xe atoms are grey.

TABLE I. DFT-MD results for the liquid ethane Hugoniot

Density (g/cm^3)	Pressure (GPa)	Energy (eV/atom)	Temperature (K)
0.571	0.4674	-5.264	163
0.800	2.290	-5.238	204
1.00	7.438	-5.137	530
1.10	11.23	-5.054	618
1.20	16.92	-4.918	947
1.30	25.30	-4.705	1487
1.40	35.44	-4.471	2175
1.50	46.98	-4.232	2876
1.60	55.71	-3.953	3142
1.70	64.50	-3.677	3386
1.80	78.20	-3.259	4043
1.906	110.3	-2.586	7000
1.929	134.7	-2.019	10000
1.942	175.0	-1.040	15000
1.95	187.4	-0.754	16669
1.964	215.8	-0.056	20000
1.993	300.8	2.044	30000
2.000	320.1	2.526	32139
2.019	390.9	4.288	40000

III. EXPERIMENTAL APPROACH AND RESULTS

To compare with the DFT simulations and to examine pure ethane and Xe-ethane mixtures at extreme conditions, we performed a series of shock and reshock experiments using Sandia's Z-Machine.[34] The Z-Machine is capable of accelerating solid aluminum flyers up to velocities of 40 km/s.[35] This technique has been used to accurately measure the Hugoniot and second shock states for several cryogenic fluids such as deuterium,[9,36] xenon,[11] and CO_2.[15] The target cell consists of two z-cut α quartz windows on the front and back of the target cell. A copper spacer is placed between the quartz win-

TABLE II. DFT-MD Hugoniot points for the 50/50 mass mixture ($x = 0.5$) of liquid Xe-ethane

Density (g/cm^3)	Pressure (GPa)	Energy (eV/atom)	Temperature (K)
0.960	0.893	-5.151	163
1.250	2.068	-5.098	214
1.500	4.270	-5.076	226
1.600	5.875	-5.043	308
1.750	9.055	-4.971	495
2.000	16.20	-4.790	1003
2.250	28.25	-4.465	1972
2.500	42.81	-4.041	2919
2.750	58.30	-3.560	3730
2.997	77.51	-2.948	5000
3.000	77.78	-2.939	5021
3.050	83.12	-2.770	5451
3.140	117.0	-1.753	10000
3.191	186.2	0.289	20000
3.231	260.2	2.492	30000
3.307	337.9	4.866	40000
3.360	421.4	7.418	50000
3.378	508.0	10.03	60000

TABLE III. DFT-MD Hugoniot points for the 50/50 molar mixture ($x = 0.19$) of liquid Xe-ethane

Density (g/cm^3)	Pressure (GPa)	Energy (eV/atom)	Temperature (K)
1.676	0.780	-4.708	163
2.500	3.257	-4.664	167
2.600	3.997	-4.646	209
2.800	5.983	-4.594	310
3.050	8.876	-4.508	500
3.250	10.64	-4.445	800
3.500	16.23	-4.264	1221
3.750	21.92	-4.062	1834
4.000	29.58	-3.783	2579
4.500	44.98	-3.173	3652
5.000	67.10	-2.266	5902
5.250	81.74	-1.655	7409
5.514	128.0	0.198	15000
5.550	142.8	0.786	17463
5.609	156.1	1.327	20000
5.742	219.0	3.855	30000
5.850	286.2	6.576	40000
6.089	442.1	13.10	60000

dows. The rear window consists of two quartz windows bonded together using Epotek 301-2 to form a top-hat. The combination of the copper spacer and the smaller diameter quartz window in the top-hat set the cryogenic liquid sample thickness. The quartz windows are anti-reflection coated to reduce Fresnel reflections at the interfaces. The target cells are connected to a liquid nitrogen cryostat[11,15] and cooled to temperature. A schematic view of the cryotarget and experimental configuration is shown in Fig. 3. Further details of the cryotarget and system can be found in Ref. 11.

Velocity interferometry (VISAR)[37] is the primary diagnostic for the shock experiments. The Sandia VISAR system consists of two dual velocity per fringe (vpf) interferometers, which allows up to four different vpf settings to be used on a single target. This eliminates 2π ambiguity in the data analysis. Typical uncertainty in the velocity records is $< 0.5\%$. As shown in the experimental schematic view (Fig. 3), the 532 nm laser used for the VISAR passes through the target cell and reflects off the aluminum flyer. The velocity of the aluminum flyer is measured up to impact with the quartz front window. The shock front generated in the quartz window at impact is reflective[38] and the shock velocity in the quartz is measured directly using the VISAR. The shock transmitted into the ethane or the Xe-ethane mixture has a reflective shock front allowing the shock velocity in the cryogenic liquid sample to be measured directly. Lastly, the shock front in the rear quartz top-hat is also reflective, from which the state in the quartz and the reshock state in the liquid sample can be determined accurately.

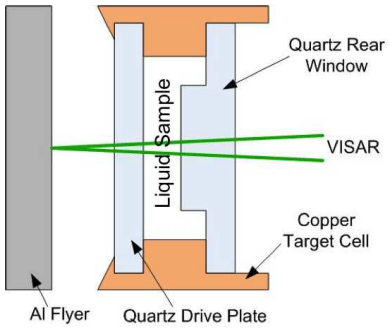

FIG. 3. Target cell configuration for the ethane and the Xe-ethane mixture shock compression experiments

The target cells were filed with high purity (>99.99%) ethane gas (Matheson TriGas) to 16.8 PSI and cooled to the final temperature. The initial density of liquid ethane was determined from the fit to the experimental data in Ref. 39 with an uncertainty of 0.5%. The index of refraction of liquid ethane was determined from the data in Ref. 40. Xe-ethane gas mixtures were supplied by Matheson TriGas and the molar ratio content was verified using mass spectrometry. The initial density of the Xe-ethane mixtures is determined from a linear fit to the experimental density data in Ref. 31. The index of refraction for the mixture was calculated using the Lorentz - Lorentz mixing rule:

$$\frac{n_{12}^2 - 1}{n_{12}^2 + 2} = \Phi_1 \frac{n_1^2 - 1}{n_1^2 + 2} + \Phi_2 \frac{n_2^2 - 1}{n_2^2 + 2} \qquad (2)$$

with

$$\Phi_i = y_i m_i/\rho_i/\sum_j y_j m_j/\rho_j.$$

where y is the molar fraction, m is the atomic mass, and ρ is the density.[41] The initial density and index of refraction values for liquid Xe were taken from the literature.[42] Since the shock velocity is measured directly, the measured shock velocities can be integrated with respect to time to ensure the distance traveled is consistent with the sample size.

The principal Hugoniot state is calculated using a *Monte Carlo* impedance matching with a cubic fit to the published quartz data[15,38] and a quartz release model based on an effective Grüneisen Γ parameter.[43] For the experiments on the mixtures, the uncertainty in the molar concentration contributes primarily to the uncertainty in initial density (up to ≈4%), while the effect on the index of refraction is small, $< 0.05\%$. The small effect on the index is primarily caused by xenon and ethane having similar indices of refraction at the experimental temperatures: at 161.5 K $n_{Xe} = 1.392$ and $n_{ethane} = 1.343$. Tables IV - IX list the experimental observables (U_S^{Quartz} and U_S^{Liquid}), the principal Hugoniot states, and the reshock states.

IV. DISCUSSION AND RESULTS

Figure 4 plots the experimental observables U_S^{Quartz} and U_S^{Liquid} for the four samples: pure Xe, 50/50 molar mixture ($x = 0.19$), 50/50 mass mixture ($x = 0.5$), and pure ethane. The results show that the Xe U_S^{Xenon} has the lowest velocity as a function of U_S^{Quartz}. The observed U_S^{Liquid} increases as the amount of ethane increases. The molar and mass mixture observable data are bounded by the pure ethane and xenon data, as expected. The observable data were fitted using the York method of linear fitting for uncertainty in X and Y direction.[44] A large change in the slope parameter occurs in the linear fits to the data between the molar and mass mixtures. That the change in the slope parameter occurs between the mass and molar mix ratios suggests that the high pressure response is governed more by the differing masses of the elements rather than the relative chemical interactions.

Figure 5 shows the compiled Hugoniot data sets for the pure and mixed liquids including the pure Xe, from Ref. 11. Tables I-III show the calculated values for points along the Hugoniot. The temperatures given in clean values, such as 40000K, were fixed when a density scaling procedure is performed. These are often the higher temperature points where the sharp rise in the Hugoniot makes temperature scaling inaccurate. Note that for ethane, we have both density and temperature scaling points interwoven suggesting that both methods are equally accurate in an intermediate region. The results from the DFT simulations show good agreement with the experimental data. For the pure ethane and the two mixtures, the Hugoniot is observed to undergo a sharp steepening after complete dissociation of the ethane. The DFT simulation results tend to show a slightly stiffer Hugoniot than the experimental results at the highest pressures. This has been observed in other comparisons with experiments[11,15] and is likely the result of the computational limits on the number of bands with ever diminishing weights required to describe the energy states.

In the High-Foot Campaign for capsule implosion, the DT fuel is compressed through a series of shocks.[4–6] Modeling of this system requires accurate equations of state with knowledge of off-principal Hugoniot behavior as well as an understanding of the EOS of mixtures. Reshock data provides additional off-Hugoniot data that can be used in the development of EOS models and also provides additional data for validating mixture models. Although we did not calculate the reshock states using DFT, the target design shown in Fig. 3, with the rear quartz top-hat, does permit the measurement of the reshock state in the ethane and mixture samples. Calculating the reshock state requires knowing the sample Hugoniot state prior to reshock. We use the method described in Ref. 15 to determine the reshock states. The method utilizes a fit to the U_S-U_P data to determine the initial state of the sample prior to reshock because some attenuation can exist in the shock velocity as the shock traverses the sample. Since we only have a few experimental points for the principal Hugoniot of ethane and the mixtures, we include the DFT data in the $U_S - U_P$ fits. We assume a 0.5% uncorrelated uncertainty in the DFT U_S-U_P data points. The final state pressure P and U_P are known to a high degree of accuracy because of the quartz Hugoniot.[38] The linear U_S-U_P parameters along with the correlation between the fit parameters used in the reshock calculation are listed in Table VII. The reshock states are listed in Tables VIII and IX. Figure 6 plots the reshock states in comparison to the DFT principal Hugoniot data and the calculated initial state. Reshock data were attained up to pressures of 8.5 Mbar. The reshock data have a larger uncertainty than the principal Hugoniot data because of uncertainty in the initial state prior to reshock. Uncertainties could be reduced with further measurements on the principal Hugoniot.

Experimentally, measuring temperature is difficult. However, temperature is a known quantity in the DFT simulations. Fig. 7 shows the DFT Hugoniot data in pressure - temperature space. For a given pressure, the shock temperature in pure Xe is noticeably higher than the pure ethane or Xe-ethane mixtures. Dissociation of the ethane absorbs energy generated in the shock, thus keeping the temperature lower. The addition of xenon means fewer dissociating ethane molecules to absorb the shock energy and higher temperature for a given pressure. Because of xenon's higher mass it moves slower on average at a given temperature than ethane. This results in less frequent collisions and resulting chemistry

TABLE IV. Experimental data of the principal Hugoniot for shock compressed liquid ethane.

Shot	Quartz U_S (km/s)	ρ_0^{Ethane} (g/cm^3)	T_0 (K)	U_P (km/s)	U_S (km/s)	ρ (g/cm^3)	P (GPa)
Z2331	17.32±0.03	0.571	162.0	14.00 ± 0.05	20.07 ± 0.03	1.888 ± 0.017	160.4 ± 0.8
Z2226	18.17±0.04	0.570	161.5	14.89 ± 0.06	21.3 ± 0.07	1.897 ± 0.024	181.1 ± 1.1
Z2277	20.52±0.04	0.572	163.5	17.40 ± 0.06	24.6 ± 0.06	1.952 ± 0.021	244.5 ± 1.4

TABLE V. Principal Hugoniot experimental data for shock compressed liquid Xe-ethane ∼50/50 mass mix ($x = 0.5$).

Shot	Quartz U_S (km/s)	ρ_0^{MIX} (g/cm^3)	T_0 (K)	U_P (km/s)	U_S (km/s)	ρ (g/cm^3)	P (GPa)
Z2527N	23.25 ± 0.07	0.958±0.021	161.5	18.61 ± 0.13	25.75 ± 0.07	3.457 ± 0.061	459.1 ± 8.1
Z2527S	24.23 ± 0.08	0.958±0.021	161.5	19.59 ± 0.14	27.08 ± 0.09	3.464 ± 0.067	508.1 ± 9.0

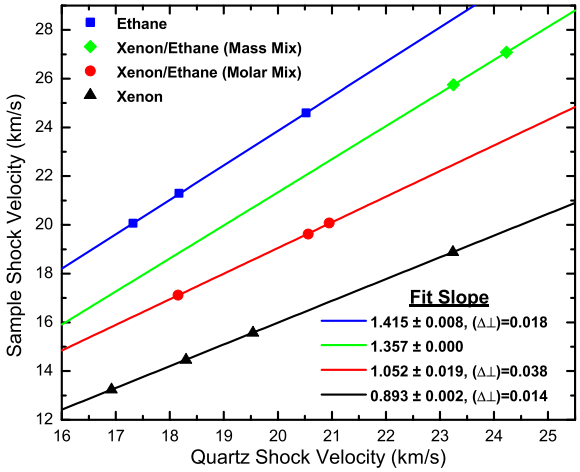

FIG. 4. Experimental measurements: quartz shock velocity (U_S^{Quartz}) vs. sample shock velocity (U_S). The data for the pure Xe is from Ref. 11. The lines are linear fits to the data. The slope uncertainty and the sum of the orthogonal distance from the fit are listed on the figure.

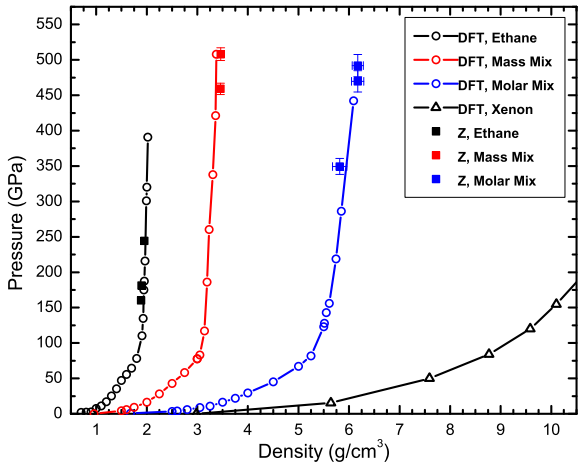

FIG. 5. Hugoniot data from the Z-experiments and the DFT simulations for the pure ethane, mass mixture, molar mixture, and pure Xe. All DFT data start from a reference state density for the system at T=163K and 0 bar pressure. The initial states for the experimental data are listed in Tables IV - VI Error bars for the experimental data are on the order of the symbol unless indicated otherwise.

for a given temperature.

The temperature data (Fig. 7) also provides indication of complete dissociation of the ethane molecules around 100 GPa where the slope in the P-T data increases. The mass mixture is mostly ethane and still exhibits the discreet regions of differing slopes in P-T before the sharp up turn. This is not evident in the molar results suggesting that the chemistry is highly affected by the 1-to-1 ratio of Xe to ethane. The inclusion of Xe also has a mollifying effect on the sharp upturn observed in ethane ρ-P Hugoniot (Fig. 5), which is a signature of dissociation completion. Both the mass and molar mixture exhibit a sharp upturn, but at slightly higher pressures and the post-dissociation Hugoniot is softer than the pure ethane.

In Fig. 8, we juxtapose the principal Hugoniot for shocked liquid ethane with the decomposition pathway of the ethane determined from the DFT simulations. Ethane decomposition starts at approximately 29 GPa and corresponding density of 1.3 g/cm^3. In terms of compression, $\mu = 1 - \rho_0/\rho$; the onset of decomposition is $\mu = 0.56$. The decomposition begins with the removal of H from the ethane molecule. Initially, the trace molecules observed are primarily C_2H_5 and C_2H_4, but can include other C-H molecules. As the shock pressure increases, the number of liberated H and the number of trace molecules increases. By 1.7 g/cm^3, most molecules have decomposed with only a few (1% to 2%) CH and CH_2 present at any given time. At pressures above 55 GPa and $\rho =$ 1.7 g/cm^3, the trace C_XH_Y molecules begin to dissociate rapidly into C and H atoms. Complete dissociation - no C_2H_6 and no trace C-C or C-H molecules occurs by 110 GPa and a density of 1.9 $g/cm^3(\mu = 0.70)$. We note that the sharp up turns in the Hugoniots do in fact correspond to complete dissociations.

Figure 9 plots the decomposition pathways for the

TABLE VI. Experimental data of the principal Hugoniot for shock compressed mixtures of a 50/50 molar mixture ($x = 0.19$) of liquid ethane and liquid xenon with an initial density of ρ=1.676 g/cm^3 .

Shot	Quartz U_S (km/s)	ρ_0^{MIX} (g/cm^3)	T_0 (K)	U_P (km/s)	U_S (km/s)	ρ (g/cm^3)	P (GPa)
Z2226	18.15 ± 0.05	1.676±0.073	163.5	12.18 ± 0.16	17.12 ± 0.09	5.814 ± 0.142	349.4 ± 11.3
Z2277	20.56 ± 0.04	1.676±0.073	163.5	14.29 ± 0.18	19.62 ± 0.08	6.171 ± 0.122	469.6 ± 15.0
Z2295	20.95 ± 0.03	1.676±0.073	163.0	14.63 ± 0.18	20.08 ± 0.07	6.173 ± 0.109	491.9 ± 15.7

TABLE VII. Linear fit parameters to the U_S-U_P experimental data and DFT results used in determining the reshock states. $U_S = C_0 + S_1 U_P$. The term $\sigma_{C_0}\sigma_{S_1}$ is the off-diagonal term in the covariance matrix of the fit parameters

	Range (km/s)	C_0 (km/s)	S_1	$\sigma_{C_0}\sigma_{S_1} \times 10^3$
Ethane	$U_S > 15.0$	1.045±0.254	1.349 ± 0.017	-4.1634
Mass Mix	$U_S > 13.0$	1.069±0.195	1.336 ± 0.014	-2.6083
Molar Mix	$U_S > 10.0$	0.929±0.127	1.313 ± 0.014	-1.7045

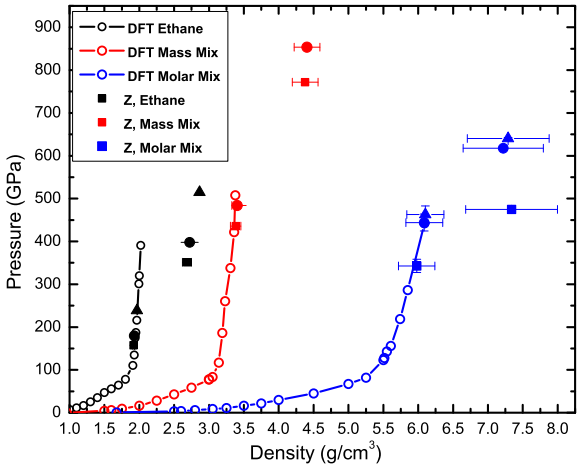

FIG. 6. Reshock data in ρ-P space for ethane and Xe-ethane mixtures. The symbols are chosen so that the principal Hugoniot state and reshock state have corresponding symbols.

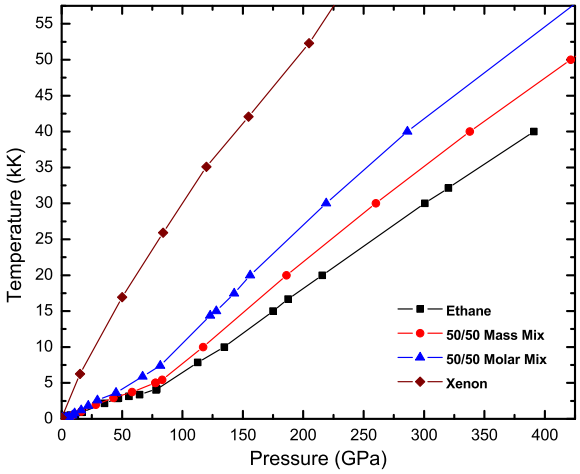

FIG. 7. DFT Hugoniot calculations in P-T space. The P-T slope increases after complete dissociation of the ethane.

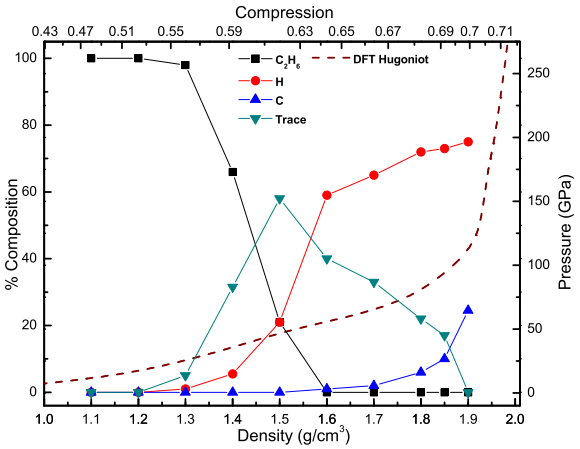

FIG. 8. The percent of total atoms in the system that are in each molecule type. The Xe atom percentage is not shown. Trace refers to all possible C-C and C-H combinations excluding C_2H_6. Juxtaposed on the plot is the DFT Hugoniot (dashed-line). Complete dissociation is observed by 1.9 g/cm^3.

mass mix ($\rho_0 = 0.960 g/cm^3$, $x = 0.50$). The onset of appreciable decomposition starts after 9 GPa and a density of 1.75 g/cm^3, which corresponds to a compression of $\mu = 0.45$. The remainder of trace molecules grows rapidly with shock pressure obtaining a maximum at 43 GPa. Above this pressure, atomic C accumulates. Decomposition is completed by 117 GPa and $\rho = 3.14 g/cm^3$. The compression at this state is $\mu = 0.69$. At this point, the Hugoniot steepens significantly as shown in Figure 9.

Figure 10 shows the decomposition pathway for the molar mixture ($\rho_0 = 1.676 g/cm^3$, $x = 0.19$). The additional Xe increases the pressure for complete dissociation to 126 GPa and a density of $5.5 g/cm^3$; this corresponds to a compression of μ=0.69 for complete dissociation. While the addition of Xe causes the complete dissociation pressure and temperature to increase slightly, the end compression state μ is the nearly same for ethane

TABLE VIII. Reshock data for liquid ethane.

Shot	Ethane U_S (km/s)	Quartz U_S (km/s)	ρ_2 (g/cm^3)	P_2 (GPa)
Z2277	24.26±0.06	18.36±0.04	2.864 ± 0.064	514.8 ± 2.7
Z2226	21.14±0.06	16.41±0.06	2.722 ± 0.068	397.9 ± 3.4
Z2331	19.81±0.05	15.54±0.05	2.684 ± 0.064	351.3 ± 2.6

TABLE IX. Reshock data for the Xe-ethane mixtures.

Shot	Mix Ratio x	Mix U_S (km/s)	Quartz U_S (km/s)	ρ_2 (g/cm^3)	P_2 (GPa)
Z2226	0.19	16.86±0.07	17.72± 0.04	7.338±0.658	474.5±2.5
Z2277	0.19	19.12±0.08	19.88± 0.05	7.219±0.575	617.9±3.7
Z2295	0.19	19.51±0.07	20.19± 0.03	7.290±0.587	640.3±2.3
Z2527 (N)	0.5	25.19±0.07	21.90± 0.09	4.379±0.185	771.8±7.4
Z2527 (S)	0.5	26.52±0.09	22.88± 0.08	4.405±0.185	853.5±7.0

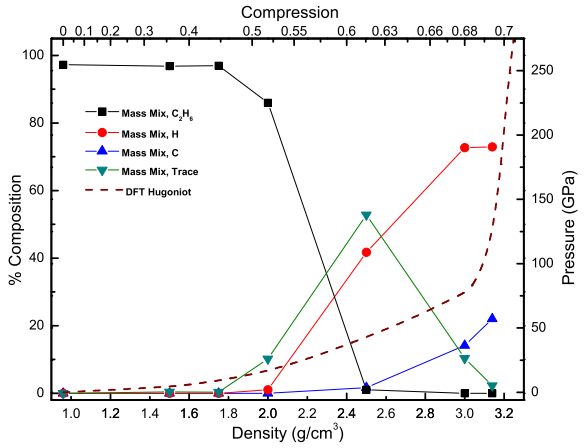

FIG. 9. Decomposition of the 50/50 mass mixture (ρ_0=0.96g/cm^3, x = 0.50) along the Hugoniot. The dashed line indicates the DFT calculated Hugoniot.

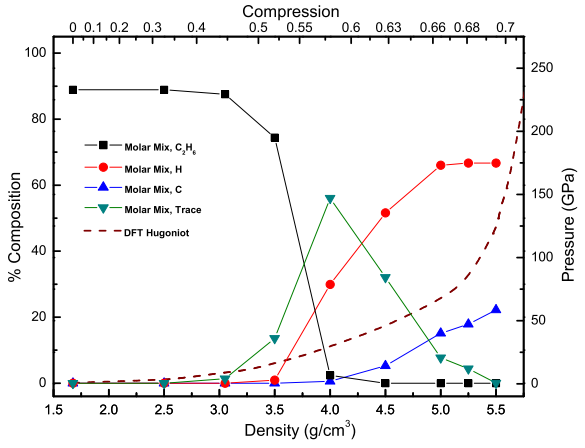

FIG. 10. Decomposition of the 50/50 molar mixture (ρ_0=1.676g/cm^3, x = 0.19) along the Hugoniot. The dashed line indicates the DFT calculated Hugoniot.

and mixtures of Xe-ethane. In neither the mass (x=0.5) nor the molar (x=0.19) mixtures did we observe the formation of any Xe bonded system (Xe-Xe, Xe-C, or Xe-H) as has been observed in other high pressure systems.[16,45] We attribute this to the high temperatures in the systems. In addition, as we show that the C-C bond has a limiting compression, it is likely that Xe-bonds have a limiting compression too.

The similar compression ratios indicates that complete dissociation for the pure ethane and Xe-ethane mixture systems has a strong dependence on the density. Interestingly, the ratio μ = 0.69 for ethane is also similar to the compression ratios for other C-C bonded systems. Polystyrene completely dissociates at μ=0.62;[46] polyethylene is completely dissociated at μ=0.62;[47] and poly 4-methyl-1-pentene (PMP) is completely dissociated at μ=0.68.[13] This suggests that a limiting compression exists for C-C bonded systems.

V. CONCLUSION

We have performed series of experimental measurements and DFT-MD simulations on ethane and Xe-ethane mixtures to understand the response of atomic mixtures at high pressures and temperatures. The experimental measurements provided accurate Hugoniot data for ethane and Xe mixtures that were used to validate DFT-MD simulations. DFT-MD is seen to provide accurate descriptions of Hugoniot state properties of dissimilar pure species as well as homogeneous mixtures of them. Further examination of the simulations showed that ethane dissociation begins with the release of bound H. As the pressure increases, ethane eventually dissociates into C and H atoms. The addition of Xe increased the pressure and temperature for complete dissociation, but the ultimate compression for dissociation of the system remained the same regardless of the Xe concentra-

tion. Since the upturn in the Hugoniot occurs at the similar compression ratios for each species, the state of complete dissociation is likely caused by a limiting compression rather than purely kinetic reasons.

Hydrodynamics simulations of high energy density physics phenomena require detailed knowledge of the EOS of the constituents and their mixtures. In ICF targets, high Z contamination can affect timing. The results in this paper provide a test case for EOS mixture models and for simulating high Z contamination influences on the EOS for ICF applications.

ACKNOWLEDGMENTS

We thank Drs. John Benage and Luke Shulenberger for valuable discussions on this work. We thank Dr. Joel Kress at Los Alamos National Laboratory for valuable discussions on mix rules and DFT-MD simulations. We thank Jesse Lynch and Nicole Cofer for assembling the cryo-targets and we thank Andrew Lopez, Keegan Shelton, and Jose Villalva for operating the cryogenics systems on Z. The NNSA Science Campaigns supported this work. Sandia National Laboratories is a multi-program laboratory managed and operated by Sandia Corporation, a wholly owned subsidiary of Lockheed Martin Corporation, for the U.S. Department of Energys National Nuclear Security Administration under contract DE-AC04-94AL85000.

[1] S. Regan *et al.*, Phys. Rev. Lett. **111**, 045001 (2013).
[2] T. Ma *et al.*, Phys. Rev. Lett. **111**, 085004 (2013).
[3] P. A. Bradley, Phys. Plasmas **21**, 062703 (2014).
[4] T. R. Dittrich *et al.*, Phys. Rev. Lett. **112**, 055002 (2014).
[5] H.-S. Park *et al.*, Phys. Rev. Lett. **112**, 055001 (2014).
[6] O. A. Hurricane *et al.*, Nature Letters **506**, 343 (2014).
[7] J. Biener *et al.*, Nucl. Fusion **52**, 062001 (2012).
[8] D. S. Clark *et al.*, Phys. Plasmas **17**, 052703 (2010).
[9] M. D. Knudson, D. L. Hanson, J. E. Bailey, C. A. Hall, J. R. Asay, and W. W. Anderson, Phys. Rev. Lett. **87**, 225501 (2001).
[10] M. D. Knudson, M. P. Desjarlais, and D. H. Dolan, Science **322**, 1822 (2008).
[11] S. Root, R. J. Magyar, J. H. Carpenter, D. L. Hanson, and T. R. Mattsson, Phys. Rev. Lett. **105**, 085501 (2010).
[12] R. D. Dick, J. Chem. Phys. **52**, 6021 (1970).
[13] T. R. Mattsson, J. M. D. Lane, K. R. Cochrane, M. P. Desjarlais, A. P. Thompson, F. Pierce, and G. S. Grest, Phys. Rev. B **81**, 054103 (2010).
[14] B. L. Sherman, H. F. Wilson, D. Weeraratne, and B. Militzer, Phys. Rev. B **86**, 224113 (2012).
[15] S. Root, K. R. Cochrane, J. H. Carpenter, and T. R. Mattsson, Phys. Rev. B **87**, 224102 (2013).
[16] M. Somayazulu, P. Dera, A. F. Goncharov, S. A. Gramsch, P. Liermann, W. Yang, Z. Liu, H. Mao, and R. J. Hemley, Nature Chem. **2**, 50 (2010).
[17] P. Hohenberg and W. Kohn, Phys. Rev. **136**, B864 (1964).
[18] W. Kohn and L. J. Sham, Phys. Rev. **140**, A1133 (1965).
[19] N. D. Mermin, Phys. Rev. **137**, A1441 (1965).
[20] G. Kresse and J. Hafner, Phys. Rev. B **47**, R558 (1993).
[21] G. Kresse and J. Hafner, Phys. Rev. B **49**, 14251 (1994).
[22] G. Kresse and J. Furthmüller, Phys. Rev. B **54**, 11169 (1996).
[23] P. E. Blöchl, Phys. Rev .B **50**, 17953 (1994).
[24] G. Kresse and D. Joubert, Phys. Rev. B **59**, 1758 (1999).
[25] A. E. Mattsson, P. A. Schultz, M. P. Desjarlais, T. R. Mattsson, and K. Leung, Modelling Simul. Mater. Sci. Eng. **13**, R1 (2005).
[26] A. Baldereschi, Phys. Rev. B **7**, 5212 (1973).
[27] M. P. Desjarlais, Phys. Rev. B **68**, 064204 (2003).
[28] R. Armiento and A. E. Mattsson, Phys. Rev. B **72**, 085108 (2005).
[29] A. E. Mattsson, R. Armiento, J. Paier, G. Kresse, J. M. Wills, and T. R. Mattsson, J. Chem. Phys. **128**, 084714 (2008).
[30] M. P. Allen and D. J. Tildesley, *Computer Simulation of Liquids* (Oxford Science Publications, 1990).
[31] E. J. M. Filipe, E. J. S. Gomes de Azeveda, L. F. Martins, V. A. Soares, and J. Calado, J. Phys. Chem B **104**, 1315 (2000).
[32] M. French and R. Redmer, Journal of Physics: Condensed Matter **21**, 375101 (2009).
[33] M. French, T. R. Mattsson, and R. Redmer, Phys. Rev. B **82**, 174108 (2010).
[34] M. E. Savage *et al.*, in *2007 IEEE Pulsed Power Conference*, Vol. 1-4 (2007) p. 979.
[35] R. W. Lemke, M. D. Knudson, D. E. Bliss, K. Cochrane, J.-P. Davis, A. A. Giunta, H. C. Harjes, and S. A. Slutz, J. Appl. Phys. **98**, 073530 (2005).
[36] M. D. Knudson, D. L. Hanson, J. E. Bailey, C. A. Hall, J. R. Asay, and C. Deeney, Phys. Rev. B **69**, 144209 (2004).
[37] L. M. Barker and R. E. Hollenbach, J. Appl. Phys. **43**, 4669 (1972).
[38] M. D. Knudson and M. P. Desjarlais, Phys. Rev. Letts. **103**, 225501 (2009).
[39] W. M. Haynes and M. J. Hiza, J. Chem. Thermodynamics **9**, 179 (1977).
[40] L. A. Weber, J. Chem. Phys. **65**, 446 (1976).
[41] R. Mehra, Proc. Indian Acad. Sci (Chem. Sci.) **115**, 147 (2003).
[42] A. J. Leadbetter and H. E. Thomas, Trans. Faraday Soc. **61**, 10 (1965).
[43] M. D. Knudson and M. P. Desjarlais, Phys. Rev. B **88**, 184107 (2013).
[44] D. York, Can. J. Phys. **44**, 1079 (1966).
[45] W. Grochala, Chem. Soc. Rev. **36**, 1632 (2007).
[46] C. Wang, X. T. He, and P. Zhang, Phys. Plasmas **18**, 082707 (2011).
[47] K. R. Cochrane, M. P. Desjarlais, and T. R. Mattsson, in *AIP Conf. Proc.*, Vol. 1426 (2012) p. 1271.